Journal of ELECTRONIC MATERIALS, Vol. 16, No. 1, 2015
DOI: 10.1007/s11664-014-3414-9

Electron Paramagnetic Resonance and Photoluminescence Studies of Ultraviolet-Emitting $ZnAl_2O_4:Gd^{3+}$ Phosphors

VIJAY SINGH,[1,5] G. SIVARAMAIAH,[2] J.L. RAO,[3] S.J. DHOBLE,[4] and S.H. KIM[1]

1.—Department of Chemical Engineering, Konkuk University, Seoul 143 701, Korea. 2.—Department of Physics, Government College for Men (Autonomous), Kadapa 516 004, India. 3.—Department of Physics, Sri Venkateswara University, Tirupati 517 502, India. 4.—Department of Physics, R.T.M. Nagpur University, Nagpur 440033, India. 5.—e-mail: vijayjiin2006@yahoo.com

Gadolinium-doped $ZnAl_2O_4$ ultraviolet-emitting powder phosphor was prepared at ~773 K within a few minutes by the combustion route. A cubic spinel structure of the as-prepared sample was confirmed by the x-ray diffraction method. The morphology and homogeneity of chemical composition of the sample were analyzed using scanning electron microscopy and energy-dispersive x-ray analysis, respectively. Electron paramagnetic resonance (EPR) and photoluminescence studies were performed on the Gd-doped $ZnAl_2O_4$ phosphors. The EPR spectrum exhibited signals with effective g values at g = 5.7, 4.4, 3.4, 2.8, 2.3, and 2.0. The signals with effective g values at g = 5.7, 2.8, and 2.0 are attributed to strong, intermediate, and weak cubic crystal fields. The signal at g = 4.4 is attributed to a strong crystal field with orthorhombic symmetry. The signals at g = 3.4 and 2.3 are attributed to the vitreous structure. The emission spectrum exhibits an intense band in the ultraviolet (UV) region centered at 312 nm (32,051 cm^{-1}), being assigned to the $^6P_{7/2} \rightarrow {}^8S_{7/2}$ transition.

Key words: Combustion, XRD, EPR, Gd^{3+} ions, $ZnAl_2O_4$, luminescence

INTRODUCTION

Research has been stimulated due to the need for new ultraviolet-emitting phosphors suitable for use in the lighting industry and other applications such as vitamin D synthesis, photochemical reactions, water purifiers, phototherapy, etc.[1–5] In the recent past, rare-earth-doped inorganic phosphor systems have attracted significant interest due to their wide range of applications in the fields of display devices, lamp phosphors, detector systems, etc.[6–10] Several groups have reported a variety of rare-earth-doped aluminate oxide phosphors showing efficient emission in the visible region.[11–14] In this family, $ZnAl_2O_4$ has been extensively characterized.[15–18] $ZnAl_2O_4$ is suggested to be an excellent host for accommodating rare-earth as well as transition-metal ions, and extensive studies have been carried out on the luminescence properties using this matrix.[19–23] $ZnAl_2O_4$ is a wide-bandgap semiconductor with optical bandgap of 3.8 eV, making it useful for photoelectronic devices.[24] In this host, most transition-metal and lanthanide ions are stabilized. According to our knowledge, there are no reports on Gd-doped $ZnAl_2O_4$ phosphors.

In recent years, $ZnAl_2O_4$ has been synthesized and well characterized.[25–28] The effects of the preparation conditions on the cathodoluminescence properties of rare-earth-doped zinc aluminate films have been studied.[29] Luminescence induced by friction, i.e., mechanoluminescence, was observed for $ZnAl_2O_4:Mn^{2+}$ fabricated by controlling the reducing temperature.[30] The cathodoluminescence properties of green-emitting $ZnAl_2O_4$:Mn thin films under low to medium excitation voltage have been investigated.[31] Barros et al.[32] prepared and characterized europium- and terbium-doped zinc

(Received January 20, 2013; accepted September 8, 2014; published online October 7, 2014)

aluminate oxide nanocrystals with spinel structure. Camargo et al.[33] reported spectroscopic investigation of upconversion emissions in $ZnAl_2O_4:Er^{3+}/Yb^{3+}$ powder samples. Electron paramagnetic resonance (EPR) and luminescence studies of $ZnAl_2O_4$:Mn phosphors were reported by Singh et al.[34] They also reported thermally stimulated luminescence and electron spin resonance investigations on gamma-irradiated Er/Yb-codoped $ZnAl_2O_4$ phosphors.[35] Menon et al.[36] investigated thermally stimulated luminescence and optically stimulated luminescence properties of Tb-doped $ZnAl_2O_4$ phosphors. Dutta et al.[37] reported synthesis of a novel composition of nanocrystalline $ZnAl_2O_4:Dy^{3+},Tb^{3+},Eu^{3+}$ phosphors which simultaneously emit blue, green, yellow, and red light. Spherical porous Eu^{3+}-doped $ZnAl_2O_4$ phosphor was prepared by a hydrothermal route.[38] Chen et al.[39] prepared $ZnAl_2O_4:Eu^{3+}$ hollow nanophosphors having high surface area and excellent red-emitting property. Manganese-doped zinc aluminate spinel phosphors have been prepared by the sol–gel process.[40] Luminescence and EPR studies of Cr^{3+} ions in $ZnAl_2O_4$ phosphor material have also been reported.[41] Tshabalala et al.[42] reported luminescent properties and x-ray photoelectron spectroscopy study of $ZnAl_2O_4:Ce^{3+}$, Tb^{3+} phosphor.

Research on trivalent gadolinium-ion-doped materials is important because these materials have great potential to be applied in the lighting industry. Gd-doped systems are plying a vital role in achieving ultraviolet (UV)-emitting phosphors. The Gd^{3+} ions were excited with UV light, and emission from Gd^{3+} ions in the phosphors takes place in the UV region. During phototherapy investigations, it was found that UV in the region of 270 nm to 300 nm is not very effective, whereas UV in the narrow region from 300 nm to 320 nm showed remarkable therapeutic effects.[2] UV emission in a narrow band centered at about 311 nm is thus required. Ultraviolet-emitting properties of Gd-doped Y_2O_3 phosphor were investigated by Abdullah et al.[5] Okamoto et al.[6] studied ultraviolet luminescence from Pr^{3+}-sensitized $LaPO_4:Gd^{3+}$ phosphor under vacuum-ultraviolet excitation. $YAl_3(BO_3)_4:Gd^{3+}$ has been suggested as an efficient ultraviolet-emitting phosphor for use in ultraviolet lamps.[10] No EPR studies of Gd^{3+} ions in $ZnAl_2O_4$ have been carried out to date. EPR data enable one to determine the local symmetry as well as accurately estimate the oxidation state of the rare-earth ions in inorganic phosphor systems. In view of this, the authors thoroughly studied the EPR spectra of Gd^{3+} ions in this system. This work is part of an ongoing effort to study the luminescent properties of aluminate oxide phosphors doped with transition-metal and rare-earth ions.

It is well known that oxide phosphors can be considered promising, efficient and stable phosphor materials. It has also been determined that it is difficult to produce complex oxide hosts using low-temperature synthesis methods because of the high melting point of these materials and unexpected compositional deviation. However, in recent years, the authors have demonstrated that self-heat-generating methods, popularly termed combustion synthesis, offer a convenient method for producing inorganic complex oxide phosphors at relatively low temperature and in short time duration.[14,43,44] In the present work, the combustion method was adopted to prepare Gd-doped $ZnAl_2O_4$ phosphor. The prepared sample was characterized by x-ray diffraction (XRD) and energy-dispersive x-ray (EDX) analysis methods. In addition, the incorporated paramagnetic impurity (i.e., Gd) was characterized by optical and EPR spectroscopy.

EXPERIMENTAL PROCEDURES

Synthesis

A powder sample of Gd-doped $ZnAl_2O_4$ phosphor was synthesized by the combustion method. In this synthesis, metal nitrates were used as oxidizer and urea as fuel. Stoichiometric compositions of metal nitrates and fuel were calculated based upon propellant chemistry. Thus, the heat of combustion is maximum for this oxidizer/fuel ratio.[45] In a typical synthesis, 1.92 g $Zn(NO_3)_2{\cdot}6H_2O$, 5 g $Al(NO_3)_3{\cdot}9H_2O$, 0.09 g $Gd(NO_3)_3{\cdot}6H_2O$, and 2.66 g CH_4N_2O were dissolved in a very minimum quantity of deionized water in a china dish with 300 ml capacity to obtain a homogeneous solution. Then the dish was introduced into a muffle furnace preheated to ~773 K. Within a few minutes the solution boiled, ignited, and produced a self-propagating flame. In general, rare-earth doping in host matrices require high temperature and long processing time. However, combustion synthesis of phosphors requires low ignition temperature and short time duration. It has been established that the reaction is self-propagating and is able to sustain this high temperature (~1773 K) for a time of about 50 s, which brings the reaction to completion and thus yields the desired products. After the combustion reaction, the dish was immediately removed from the furnace. The products obtained by the combustion process were fluffy masses, and these were crushed into a fine powder using a pestle and mortar. This powder was further used for characterization.

Characterization

The phase composition of the synthesized powder was analyzed by XRD using a Bruker D8 advance powder diffractometer (Cu K_α radiation) in the 2θ range from 15° to 80°. The chemical compositions were analyzed using EDX attached to the SEM (S-3200 N; Hitachi, Japan). The room-temperature photoluminescence (PL) spectrum of the prepared phosphor was obtained using a Hitachi F-4500 FL spectrophotometer with a xenon lamp as excitation source. A powdered sample of 10^{-4} kg was taken in a quartz tube for EPR measurements. The EPR

spectra of all samples were recorded on a JEOL FE1X electron spin resonance (ESR) spectrometer, operating in the X-band frequencies with field modulation of 100 kHz.

RESULTS AND DISCUSSION

X-ray Diffraction

The XRD pattern of the as-prepared Gd-doped $ZnAl_2O_4$ sample is shown in Fig. 1. The diffraction pattern of the as-prepared material is very similar to the standard cubic spinel phase of $ZnAl_2O_4$ [Joint Committee on Powder Diffraction Standards (JCPDS) file no. 82-1043]. With the exception of a weak unidentified XRD peak at 34.5°, all the peak positions are in accordance with the standard cubic spinel structure of $ZnAl_2O_4$. A weak unidentified XRD peak at 34.6° was also reported elsewhere.[23] The presence of ZnO secondary phase was also observed in the rare-earth-doped $ZnAl_2O_4$ phosphor.[32] However, it is worth noting that the cubic spinel phase could be obtained even at furnace temperature as low as 773 K using combustion synthesis. Compared with the conventional solid-state method, a much lower furnace temperature was used to obtain $ZnAl_2O_4$ cubic spinel phase.

SEM and EDX

A SEM image of the as-prepared Gd-doped $ZnAl_2O_4$ sample is shown in Fig. 2a, taken in backscattered electron detection mode. As can be seen, the crystallites do not exhibit uniform size or shape. This nonuniformity in size and shape is believed to be related to the nonuniform distribution of temperature and mass flow in the combustion flame during the combustion reaction. Some particles exhibit porosity. This could be expected due to the evolution of large amounts of gas during the combustion process. For EDX mapping and spectrum analyses, the entire area of the micrographs (Fig. 2a) was analyzed. Figure 2b shows the EDX spectrum of the Gd-doped $ZnAl_2O_4$ phosphor. Gd, Zn, Al, and O peaks are clearly recognized in the Gd-doped $ZnAl_2O_4$ phosphor. It is worth noting that the dopant element (i.e., Gd) results in several peaks of sufficient intensity. It is clear from the EDX spectrum that combustion synthesis is capable of introducing molecular-level doping into the host matrix. Figure 2c shows the elemental mapping of Gd, Zn, Al, and O for Gd-doped $ZnAl_2O_4$ phosphor. These mappings show homogeneous distribution of each element in the as-prepared phosphor. It can be seen that the embedded Gd was uniformly distributed throughout the host ($ZnAl_2O_4$) matrix even for low doping concentration. From the EDX mapping and spectrum, it can be concluded that the dopant is well dispersed in the $ZnAl_2O_4$ matrix.

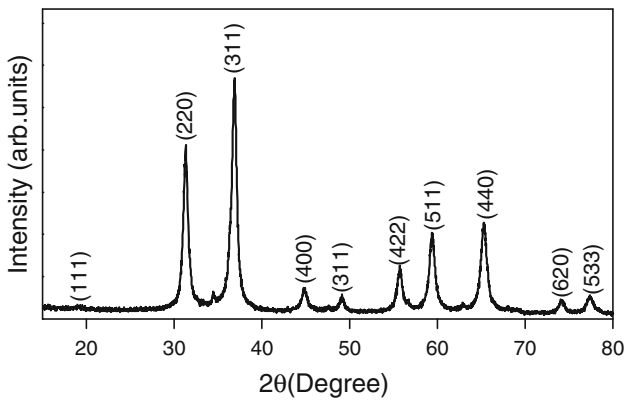

Fig. 1. Powder XRD pattern of $ZnAl_2O_4:Gd^{3+}$ phosphor.

Electron Paramagnetic Resonance Studies

Figure 3a shows the EPR spectrum of Gd-doped $ZnAl_2O_4$ phosphor recorded at 296 K. This spectrum exhibits several resonance signals with effective g values at $g = 5.7$, 4.4, 3.4, 2.8, 2.3, and 2.0. Figure 3b shows a similar spectrum recorded at 110 K, exhibiting effective g values at $g = 5.7$, 4.4, 3.4, 2.8, and 2.0. The three resonance signals at $g = 5.7$, 2.8, and 2.0 are the features of the U spectrum located at sites of strong, intermediate, and weak cubic-symmetry fields with coordination number higher than six.[46,47] The signals situated at $g = 3.4$ and 2.3 are characteristic of vitreous materials.[48] The signal at $g = 4.4$ has been attributed to strong crystal field with orthorhombic symmetry and is associated with gadolinium ions with coordination number lower than six.[49,50]

It is obvious that oxygen, which becomes nonbridging and acquires negative electrical charge, will move closer to the connected gadolinium, consequently reducing the positive electrical charge on the gadolinium. The broad EPR signal at $g = 2.0$ at 110 K could derive from interacting clustered Gd^{3+} ions linked through oxygen bridges with strong magnetic dipolar interactions.[51] The g values are invariant when the temperature is decreased from 296 K to 110 K. This elucidates that the structural environment of Gd^{3+} ions in the amorphous $ZnAl_2O_4$ matrix is invariant with temperature. One important difference between the ESR spectra obtained at 296 K and 110 K is that the signal at $g = 2.3$ which was present at 296 K is absent at 110 K. The linewidth of the signal at $g = 5.7$ decreases when the temperature is increased from 110 K to 296 K, which has been attributed to spin–spin interaction.[41]

Number of Spins

The population difference between the Zeeman levels (N) can be calculated from comparison of the area under the absorption curve with that of a standard ($CuSO_4{\cdot}5H_2O$) of known concentration. Weil and Bolton[52] gave the following formula including the experimental parameters of both the sample and the standard:

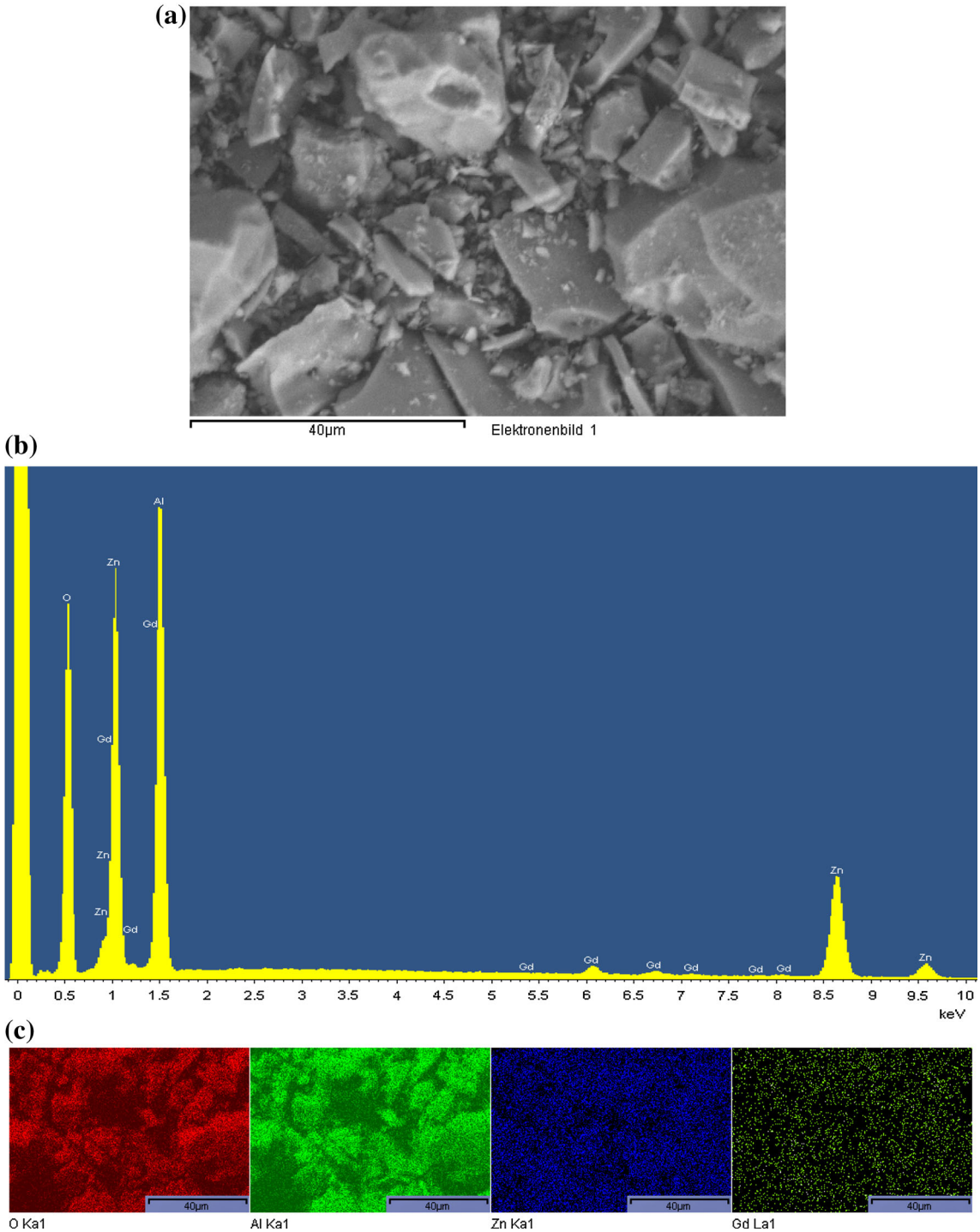

Fig. 2. (a) SEM image, (b) EDX spectrum and (c) mapping of $ZnAl_2O_4:Gd^{3+}$ phosphor.

$$N = \frac{A_x(scan_x)^2 G_{std}(B_m)_{std}(g_{std})^2[S(S+1)]_{std}(N_{std})}{A_{std}(scan_{std})^2 G_x(B_m)_x(g_x)^2[S(S+1)]_x}, \quad (1)$$

where A is the area under the absorption curve, *scan* is the magnetic field corresponding to unit length of the spectrum, G is the receiver gain (amplitude), B_m is the modulation amplitude, g is the g factor, S is the spin of the ions in the ground state (S = 7/2 for Gd^{3+} ions and 1/2 for Cu^{2+} ions). The subscripts "x" and "std" denote the sample and standard, respectively. N_{std} denotes the number of spins per kg of $CuSO_4{\cdot}5H_2O$ standard. The number

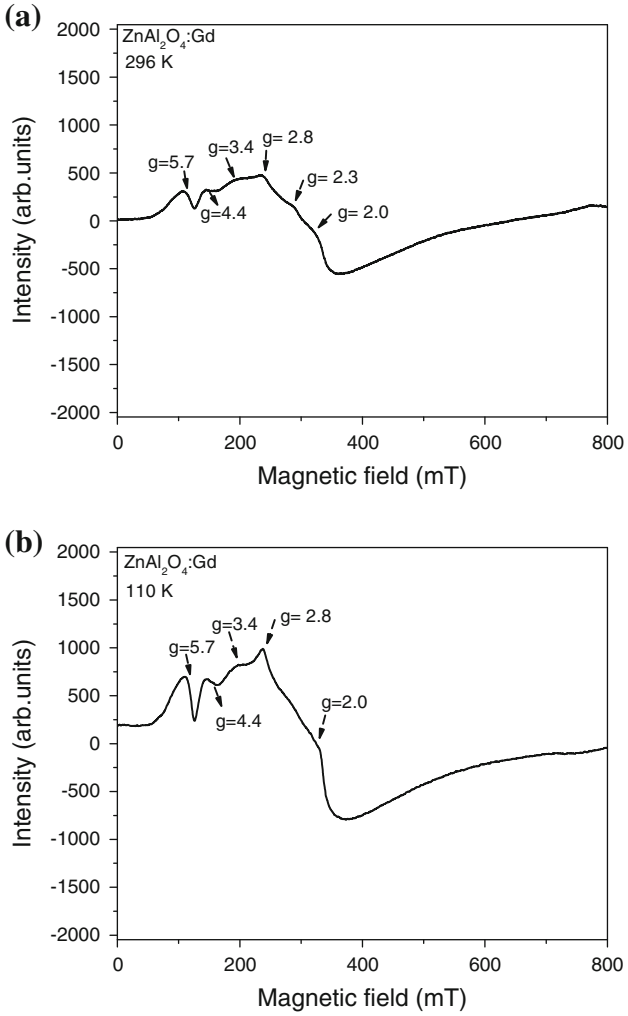

Fig. 3. EPR spectra of $ZnAl_2O_4:Gd^{3+}$ phosphor at (a) 296 K and (b) 110 K.

of spins for Gd-doped $ZnAl_2O_4$ phosphor was determined as 4.8×10^{20}/kg and 1.7×10^{20}/kg at 110 K and 296 K, respectively. The number of spins increases with the decrease of temperature in accordance with the Boltzmann distribution law.

Gibbs Energy

The Gibbs energy can be determined using the expression[53,54]

$$\Delta G = 2.303RT \log_{10}(k_B T/\lambda h), \quad (2)$$

where ΔG is the Gibbs energy or Gibbs free energy change or Gibbs energy of activation at any moment, R is the universal gas constant (8.31 J/K/mol), k_B is the Boltzmann constant (1.38×10^{-23} J/K), T is the absolute temperature, λ is the rate constant (equal to the number of spins per m^3), and h is Planck's constant (6.63×10^{-34} J s). The Gibbs energy of the Gd-doped $ZnAl_2O_4$ phosphor at g = 5.7 was found to be −47.86 kJ/mol and −19.63 kJ/mol at 296 K and 110 K, respectively. The $\log_{10}$ in the parenthesis is dimensionless. Thus, the units of ΔG are the units of RT (kJ/mol). These calculated values are consistent with values reported for glasses and minerals.[55,56] The Gibbs energy is calculated for the magnetic component of the sample. The Gibbs free energy change (ΔG) equation was taken from another form of the Arrhenius equation.[54] In the Arrhenius equation, the rate constant λ is equal to the number of spins per m^3. The Gibbs energy is not calculated with respect to a standard or reference here. The absolute spins are calculated with respect to a standard or reference. This is a kind of energy like an activation energy. The negative sign indicates that there may be strong attractive interaction between the dopant and the phosphor lattice. The negative sign also indicates that the reaction among Gd^{3+} ions is spontaneous. The Gibbs energy increases by 28.23 kJ/mol when the temperature increases from 110 K to 296 K. This is an excellent line of evidence for chemical reactions among Gd^{3+} ions in this phosphor. The Gibbs energy is a kind of thermodynamic and chemical potential that measures the stability of a magnetic system. The Gibbs energy is lower at 296 K, indicating that the stability of this phosphor is maximum at this temperature. The temperature dependence of the Gibbs energy of this phosphor indicates that strong dipolar coupling is present between Gd^{3+} ion pairs.[53]

Magnetic Susceptibility

The magnetic susceptibility can be determined using the expression[57]

$$\chi = \frac{Ng^2\beta^2 J(J+1)}{3k_B T}, \quad (3)$$

where N is the number of spins per m^3, g is the g factor = 1.98, β is the Bohr magneton, J is the total angular momentum quantum number, k_B is the Boltzmann constant, and T is the absolute temperature. The magnetic susceptibility of Gd-doped $ZnAl_2O_4$ phosphor at 296 K and 110 K was found to be 6.2×10^{-4} m^3/kg and 4.7×10^{-3} m^3/kg, respectively. The magnetic susceptibility decreases by one order when the temperature increases from 110 K to 296 K.

Curie Constant

The Curie constant C can be found using the expression[57]

$$C = \frac{Ng^2\beta^2 J(J+1)}{3k_B}, \quad (4)$$

where the symbols have their usual meanings. The Curie constant of Gd-doped $ZnAl_2O_4$ phosphor was found to be 0.51 emu/mol and 0.18 emu/mol at 110 K and 296 K, respectively. The low Curie constant value at both temperatures indicates that high antiferromagnetic interactions are found in this phosphor.[56] This may be attributed to the

Table I. g values, zero-field splitting parameter (D), number of spins (N), Gibbs potential (ΔG), magnetic susceptibility (χ), Curie constant (C), Curie temperature (θ), and effective magnetic moment (μ_{eff}) for $ZnAl_2O_4:Gd^{3+}$ phosphor at 296 K and 110 K

T (K)	g value	D (mT)	N (spins/kg)	ΔG (kJ/mol)	χ (m^3/kg)	C (emu/mol)	θ	μ_{eff} (μ_B)
296	5.7	36.2	1.7×10^{20}	−47.86	6.2×10^{-4}	0.18	6	2.2
110	5.7	37.4	8×10^{20}	−19.63	4.7×10^{-3}	0.51	0.5	2.3

formation of Gd^{3+}–Gd^{3+} ion pairs if the exchange coupling between these ions is antiferromagnetic in nature, which is expected to result in a reduction of the Curie constant.[56]

Curie Temperature

The Curie temperature is determined using the expression[57]

$$\chi = \frac{C}{T - \theta}, \tag{5}$$

where θ is the Curie temperature, and C and T have their usual meanings. The Curie temperature for Gd-doped $ZnAl_2O_4$ phosphor is found to be 0.5 K and 6 K at 110 K and 296 K, respectively. The Curie temperature is positive and low, which could be expected for paramagnetic metal ions. The Curie temperature is a rough indicator of both the strength of the interaction between the magnetic moments and the number of magnetic ions participating in the interactions.

Experimental Effective Magnetic Moment

The experimental effective magnetic moment can be estimated using the expression[55]

$$\mu_{eff} = \frac{\sqrt{3k_B C}}{\sqrt{N}}, \tag{6}$$

where the symbols have their usual meanings. The theoretical magnetic moment value for Gd^{3+} is $7.9\mu_B$. The experimental value is found to be $2.3\mu_B$ and $2.2\mu_B$ at 110 K and 296 K, respectively. The experimental value is less than the theoretical value. This indicates that antiferromagnetic interactions are found in this phosphor.[58] In the GaN:Gd system, the estimated average value of the magnetic moment per Gd ion obtained was as high as 500 times that of the Gd atomic value. It has been argued that the enhancement of the average magnetic moment resulted from a strong contribution of the GaN host lattice to the macroscopic magnetization of the whole material.[59] Lipinska et al.[60] carried out PL and EPR studies on bulk GaN doped with Gd, detecting no ferromagnetism in the sample.

Zero-Field Splitting Parameter

The zero-field splitting parameter (D) can be calculated using the expression $D \approx \Delta B/6$, where ΔB is the linewidth between the central line and the edge line of the lower magnetic field in the EPR spectrum, being valid for first-order perturbation theory.[41] The calculated D value is found to be 36.2 mT and 37.4 mT at 296 K and 110 K, respectively. Singh et al.[41] reported a D value of 36.23 mT for Gd^{3+} ions in Y_2O_3:Gd phosphors. The zero-field splitting (zfs) arises due to the combined action of spin–orbit and electronic spin–spin coupling taken as a perturbation on the crystal field states. The zfs is the removal of the spin microstate degeneracy for systems with $S > 1/2$ in the absence of an applied field. Table I presents the

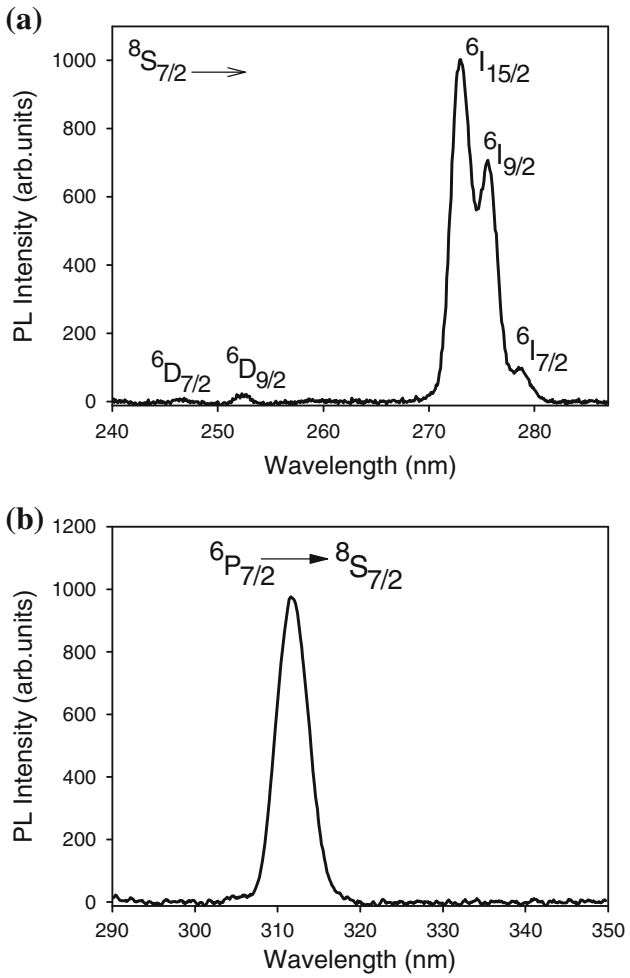

Fig. 4. Photoluminescence spectra of $ZnAl_2O_4:Gd^{3+}$ phosphor: (a) excitation spectrum of $ZnAl_2O_4:Gd^{3+}$ (λ_{em} = 312 nm) and (b) emission spectrum of $ZnAl_2O_4:Gd^{3+}$ (λ_{ex} = 273 nm).

Table II. Observed band positions for $ZnAl_2O_4$:Gd^{3+} along with their assignments

Transition from $^8S_{7/2}$ →	Observed Band Positions	
	Wavelength (nm)	Wavenumber (cm^{-1})
$^6I_{7/2}$ [62–64]	279	35,842
$^6I_{9/2}$ [62–64]	276	36,232
$^6I_{15/2}$ [62–64]	273	36,630
$^6D_{9/2}$ [62–64]	253	39,526
$^6D_{7/2}$ [62–64]	246	40,650

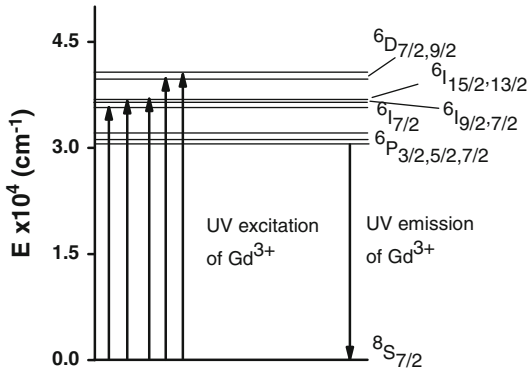

Fig. 5. Energy level diagram of Gd^{3+} ions.

g values, zero-field splitting parameter, number of spins, Gibbs energy, magnetic susceptibility, Curie constant, Curie temperature, and effective magnetic moment values observed at 110 K and 296 K for Gd-doped $ZnAl_2O_4$ phosphor.

Photoluminescence Studies

Figure 4a shows the excitation spectrum of Gd-doped $ZnAl_2O_4$ phosphor recorded at emission wavelength of λ_{em} = 312 nm. The spectrum exhibits two intense bands at around 273 nm (36,630 cm^{-1}) and 276 nm (36,232 cm^{-1}). The spectrum also exhibits three weak bands at around 246 nm (40,650 cm^{-1}), 253 nm (39,526 cm^{-1}), and 279 nm (35,842 cm^{-1}). These bands can be ascribed to Gd^{3+}:$4f^7$–$4f^7$ intraconfigurational transitions between the $^8S_{7/2}$ ground state and ^6I_J and ^6D_J excited states. In the present case, the ^6P_J and ^6G_J excited states are not observed. The observed band positions and their assignments are given in Table II. The observed band positions are consistent with the band positions reported for Gd^{3+} in materials.[61–63] All the observed band positions are in the UV region. The energy gap between the ground state $^8S_{7/2}$ and the first excited state $^6P_{7/2}$ is 32,000 cm^{-1}. Theoretical calculations show that the $4f^7$ energy levels of Gd^{3+} ion extend up to 150,000 cm^{-1}. However, energy levels up to 67,000 cm^{-1} have been reported experimentally.[64] Figure 4b shows the emission spectrum of Gd-doped $ZnAl_2O_4$ phosphor recorded at excitation wavelength of λ_{ex} = 273 nm. The spectrum exhibits an intense band in the UV region at 312 nm (32,051 cm^{-1}). This band results from transition between the first excited state ($^6P_{7/2}$) and ground state ($^8S_{7/2}$) of Gd^{3+}.[41,61–63] Figure 5 shows the energy level diagram for Gd^{3+} ion in $ZnAl_2O_4$ phosphor. From this figure, it is observed that the energy levels ^6P_J and ^6I_J are closely spaced. Josepha et al.[65] observed two peaks at 767 nm and 1536 nm for Gd^{3+} ions in TiO_2. The second peak is observed to be a multiple of the first and hence can be considered as a harmonic. The ^6I_J to ^6G_J transitions give rise to the 767 nm emission from Gd^{3+} ions.[65] The EPR effort clarifies the ground-state properties of Gd^{3+} ions, whereas the photoluminescence studies describe the excited-state properties of Gd^{3+} ions in this phosphor. EPR and optical analyses of the sample confirm the same oxidation state (i.e., 3+) of Gd in the $ZnAl_2O_4$ matrix.

CONCLUSIONS

Gd-doped $ZnAl_2O_4$ phosphor was prepared by using the solution combustion method. The XRD pattern indicated cubic spinel structure of the phosphor. SEM imaging of this phosphor indicated that the crystallites do not have uniform size or shape. From EDX mapping and spectra, it is observed that the dopant is well dispersed in the phosphor lattice. The EPR spectra of Gd-doped $ZnAl_2O_4$ phosphor exhibit signals characteristic of Gd^{3+} ions located in cubic, intermediate and strong crystal fields. The *g* values are independent of temperature variation. The Gibbs energy decreases with the decrease of temperature from 296 K to 110 K, following the usual Boltzmann law. The emission spectrum exhibits an intense narrow UV emission band at 312 nm ($^6P_{7/2}$ → $^8S_{7/2}$), which could be suitable for production of phototherapy lamps.

ACKNOWLEDGEMENTS

V.S. expresses his thanks to Konkuk University, Seoul (South Korea) for providing an Associate Professorship from the KU Research Professor Program. V.S. also expresses his thanks to Emeritus Professor Dr. Lark Kyo Kim, College of Engineering, Konkuk University, Seoul for his constant encouragement. J.L.R. thanks the University Grants Commission, New Delhi for the award of an Emeritus Fellowship.

REFERENCES

1. H.A. Klasens, A.H. Hoekstra, and A.P.M. Cox, *J. Electrochem. Soc.* 104, 93 (1957).
2. J.A. Parrish and K.F. Jacnicke, *J. Invest. Dermatol.* 76, 359 (1981).
3. L. Scherschun, J.J. Kim, and W.H. Lim, *J. Am. Acad. Dermatol.* 44, 999 (2001).
4. D.S. Thakare, S.K. Omanvar, P.L. Muthal, S.M. Dhopte, V.K. Kondawar, and S.V. Moharil, *Phys. Status Solidi A* 201, 574 (2004).

5. Mikrajuddin. Abdullah, Khairurrijal, Widayani. Sutrisno, Iis. Nurhasanah, and Aunuddin.S. Vioktalamo, *Powder Technol.* 183, 297 (2008).
6. Shinji. Okamoto, Rika. Uchino, Keisuke. Kobayashi, and Hajime. Yamamoto, *J. Appl. Phys.* 106, 013522 (2009).
7. Xigang. Wang, Du. Fuping, Donglei. Wei, Yanlin. Huang, and Hyo.Jin. Seo, *Sens. Actuators B* 158, 171 (2011).
8. F. Wang and X. Liu, *Compr. Nanosci. Technol.* 1, 607 (2011).
9. Yu. Hong, Wenwen. Zi, Shi. Lan, Shucai. Gan, Haifeng. Zou, Xu. Xuechun, and Guangyan. Hong, *Opt. Laser Technol.* 44, 2306 (2012).
10. H. Yoshida, R. Yoshimatsu, S. Watanabe, and K. Ogasawara, *Jpn. J. Appl. Phys. Part 1* 45, 146 (2006).
11. Hee.-Suk. Roh, In.-Sun. Cho, An. Jae-Sul, Chin.Moo. Cho, Tae.Hoon. Noh, Dong.Kyun. Yim, Dong.-Wan. Kim, and Kug.Sun. Hong, *Ceram. Int.* 38, 443 (2012).
12. M. Ayvacıklı, A. Ege, and N. Can, *Opt. Mater.* 34, 138 (2011).
13. Cong. Zhao, Dachuan. Zhu, Mingxing. Ma, Tao. Han, and Tu. Mingjing, *J. Alloys Compd.* 523, 151 (2012).
14. Vijay. Singh, R.P.S. Chakradhar, J.L. Rao, and Ho-Young. Kwak, *J. Lumin.* 131, 247 (2011).
15. T. Omata, N. Veda, K. Veda, and H. Kawazoe, *Appl. Phys. Lett.* 64, 1077 (1994).
16. S.K. Sampath, D.G. Kanhere, R. Randey, and J. Phys, *Condens. Matter* 11, 3635 (1999).
17. W. Strek, P. Deren, A. Bednarkiewicz, M. Zawadzki, and J. Wrzyszcz, *J. Alloys Compd.* 300–301, 456 (2000).
18. M. Zawadzki, J. Wrzyszcz, W. Strek, and D. Hreniak, *J. Alloys Compd.* 323–324, 279 (2001).
19. R. Shamsudin and R.J. Hand, *Br. Ceram. Trans.* 100, 55 (2001).
20. Hiroaki. Matsui, Xu. Chao-Nan, and Hiroshi. Tateyama, *Appl. Phys. Lett.* 78, 1068 (2001).
21. Seongwoo. Yoo, Un.-Chul. Paek, and Won.-Taek. Han, *J. Non-Cryst. Solids* 315, 180 (2003).
22. M. García-Hipólito, C.D. Hernández-Pérez, O. Alvarez-Fregoso, E. Martínez, J. Guzmán-Mendoza, and C. Falcony, *Opt. Mater.* 22, 345 (2003).
23. K.G. Tshabalala, S.H. Cho, J.K. Park, Shreyas.S. Pitale, I.M. Nagpure, R.E. Kroon, H.C. Swart, and O.M. Ntwaeaborwa, *J. Alloys Compd.* 509, 10115 (2011).
24. S.K. Sampath and J.F. Cordaro, *J. Am. Ceram. Soc.* 81, 649 (1998).
25. Robert. Ianoş, Radu. Lazău, Ioan. Lazău, and Cornelia. Păcurariu, *J. Eur. Ceram. Soc.* 32, 1605 (2012).
26. Marauo. Davis, Cenk. Gümeci, Ryan. Alsup, Carol. Korzeniewski, and Louisa.J. Hope-Weeks, *Mater. Lett.* 73, 139 (2012).
27. Diana. Visinescu, Bogdan. Jurca, Adelina. Ianculescu, and Oana. Carp, *Polyhedron* 30, 2824 (2011).
28. Adrian. Goldstein, Yehoshua. Yeshurun, Marina. Vulfson, and Haim. Kravits, *J. Am. Ceram. Soc.* 95, 879 (2012).
29. Zhidong. Lou and Jianhua. Hao, *Thin Solid Films* 450, 334 (2004).
30. Hiroaki. Matsui, Xu. Chao-Nan, Yun. Liu, and Hiroshi. Tateyama, *Phys. Rev. B* 69, 235109 (2004).
31. Z. Lou and J. Hao, *Appl. Phys. A* 80, 151 (2005).
32. B.S. Barros, P.S. Melo, R.H.G.A. Kiminami, A.C.F.M. Costa, G.F. de Sá, and S. Alves Jr., *J. Mater. Sci.* 41, 4744 (2006).
33. A.S.S. de Camargo, L.A.O. Nunes, J.F. Silva, A.C. FMCosta, B.S. Barros, J.E.C. Silva, G.F. de Sá, and S. Alves Jr., *J. Phys.: Condens. Matter* 19, 246209 (2007).
34. Vijay. Singh, R.P.S. Chakradhar, J.L. Rao, and Dong-Kuk. Kim, *J. Lumin.* 128, 394 (2008).
35. Vijay. Singh, S. Watanabe, T.K. Gundu Rao, J.F.D. Chubaci, Isabelle. Ledoux-Rak, and Ho-Young Kwak, *Appl. Phys. B* 98, 165 (2010).
36. Sanjeev. Menon, Bhushan. Dhabekar, E. Alagu Raja, S.P. More, T.K. Gundu Rao, and R.K. Kher, *J. Lumin.* 128, 1673 (2008).
37. Dimple.P. Dutta, R. Ghildiyal, and A.K. Tyagi, *J. Phys. Chem. C* 113, 16954 (2009).
38. Xiang.Ying. Chen and Chao. Ma, *Opt. Mater.* 32, 415 (2010).
39. Xiang.Ying. Chen, Ma. Chao, Shi.Ping. Bao, and Zhao. Li, *J. Colloid Interface Sci.* 346, 8 (2010).
40. Mu.-Tsun. Tsai, Yu.-Xiang. Chen, Pei.-Jane. Tsai, and Yen.-Kai. Wang, *Thin Solid Films* 518, e9 (2010).
41. Vijay. Singh, R.P.S. Chakradhar, J.L. Rao, and Ho.-Young. Kwak, *J. Mater. Sci.* 46, 2331 (2011).
42. K.G. Tshabalala, S.-H. Cho, J.-K. Park, Shreyas.S. Pitale, I.M. Nagpure, R.E. Kroon, H.C. Swart, and O.M. Ntwaeaborwa, *Phys. B* 407, 1489 (2012).
43. Vijay. Singh, R.P.S. Chakradhar, J.L. Rao, and Ho-Young. Kwak, *J. Lumin.* 131, 1714 (2011).
44. Vijay. Singh, S. Watanabe, T.K. Gundu Rao, and I.-J. Lee, *Appl. Phys. B* 104, 1019 (2011).
45. S.R. Jain, K.C. Adiga, and V.R. Pai Vernekar, *Combust. Flame* 40, 71 (1981).
46. S. Rada, V. Dan, M. Rada, and E. Culea, *J. Non-Cryst. Solids* 356, 474 (2010).
47. D.L. Griscom, *J. Non-Cryst. Solids* 40, 211 (1980).
48. I.E. Iton, C.M. Brodbeck, S.L. Suib, and G.D. Stucky, *J. Chem. Phys.* 79, 1185 (1983).
49. I. Ardelean and Lidia. Griguta, *J. Non-Cryst. Solids* 353, 2363 (2007).
50. S. Simon, I. Ardelean, S. Filip, I. Bratu, and I. Cosma, *Solid State Commun.* 116, 83 (2000).
51. T. Taurines and B. Boizot, *J. Non-Cryst. Solids* 357, 2723 (2011).
52. J.A. Weil and J.R. Bolton, *Electron Paramagnetic Resonance: Elementary Theory and Practical Applications* (New York: Wiley, 2007).
53. Gobburu. Sivaramaiah and Yuanming. Pan, *Phys. Chem. Miner.* 39, 515 (2012).
54. Wigner, Eyring, Polanyi, and Evans, *Trans. State Theory Chem. React.* (1930).
55. G. Sivaramaiah and J.L. Rao, *Spectrochim. Acta Part A* 98, 105 (2012).
56. Gobburu. Sivaramaiah, Jinru. Lin, and Yuanming. Pan, *Phys. Chem. Miner.* 38, 159 (2011).
57. A.J. Dekker, *Solid State Physics* (Groningen: Department of Electrical Engineering, University of Groningen, 2006).
58. T. Ristoiu, E. Culea, and I. Bratu, *Mater. Lett.* 41, 135 (1999).
59. S. Dhar, O. Brandt, M. Ramsteiner, V.F. Sapega, and K.H. Ploog, *Phys. Rev. Lett.* 94, 037205 (2005).
60. Z. Lipinska, M. Pawlowski, H. Zolnierowicz, A. Wysmolek, M. Palczewska, M. Kaminska, A. Twardowski, M. Bockowski, and I. Grzegory, *Acta Phys. Pol. A* 110, 243 (2006).
61. K. Binnemans, C. Görller-Walrand, and J.L. Adam, *Chem. Phys. Lett.* 280, 333 (1997).
62. P.J. Alonso, V.M. Orera, R. Cases, R. Alcalá, and V.D. Rodríguez, *J. Lumin.* 39, 275 (1988).
63. W.T. Carnall, P.R. Fields, and K. Rajnak, *J. Chem. Phys.* 49, 4412 (1968).
64. R.T. Wegh, H. Donker, and A. Meijerink, *Phys. Rev. B* 56, 13841 (1997).
65. Lyjo.K. Josepha, K.R. Dayas, Soniya. Damodarb, K. Bindu Krishnana, K. Krishnankutty, V.P.N. Nampooria, and P. Radhakrishnana, *Spectrochim. Acta Part A* 71, 1281 (2008).